Location of the Retinal of Bacteriorhodopsin's M_{412} Intermediates by Phase Modulation of Resonance Energy Transfer†

C. A. Hasselbacher, D. K. Preuss, and T. G. Dewey*
Department of Chemistry, University of Denver, Denver, Colorado 80208
Received March 25, 1985

ABSTRACT: A novel application of modulation excitation spectroscopy has been used to measure the position of the retinal chromophore in the M_{412} intermediates of the bacteriorhodopsin photocycle. This technique uses phase modulation of fluorescence resonance energy transfer to determine the distance from a lipid fluorescent donor to the chromophore of a reaction intermediate in a membrane protein. In this study, bacteriorhodopsin was incorporated into asolectin vesicles labeled with a fluorescent lipid probe. Energy transfer was measured from the fluorescent probes on the surface of the membrane to the retinal in the M_{412} intermediates. Concentrations of M_{412} intermediates in these vesicles were varied by changing the frequency of modulation of the actinic light that drives the photocycle. Simultaneous measurements of the M_{412} absorbance and of the fluorescence quenching due to resonance energy transfer were made with phase-sensitive detection. In each case, the signal amplitude decay was biphasic, indicating the presence of two M_{412} intermediates. Distances were found for each intermediate from the outer vesicle surface and from both vesicle surfaces. From this information, the distance from each membrane surface to each M_{412} intermediate could be determined. Our results show that the chromophore in the slow-decaying M_{412} intermediate is located farther from the vesicle exterior than the chromophore in the fast-decaying M_{412} intermediate. Because bacteriorhodopsin reconstitutes into these vesicles in the opposite orientation as in the native membrane, this indicates that in the intact cell the retinal in the slow M_{412} intermediate is located farther from the cytoplasmic surface than the retinal in the fast M_{412} intermediate. Implications of these results for the proton-pumping mechanism of bacteriorhodopsin are discussed.

Bacteriorhodopsin and its photocycle have been the subject of numerous investigations in recent years. This membrane-bound protein provides a relatively simple system for investigating primary events in photosynthesis and ion transport. Despite the extensive work on bacteriorhodopsin, the molecular and kinetic details of the light-driven proton-pumping process remain unresolved. Structural characterization of the intermediates is a prerequisite for a detailed understanding of the photocycle at a molecular level.

Characterization of the M_{412} intermediate has retained special interest because proton translocation has been shown to occur on a comparable time scale as M_{412} formation (Lozier et al., 1975, 1976). Also, the Schiff base linking retinal to the apoprotein in the M_{412} intermediate is deprotonated, in contrast to that of ground-state bacteriorhodopsin (Lewis et al., 1974; Mendelsohn, 1976; Aton et al., 1977; Campion et al., 1977). The M_{412} intermediate is considered likely to play a key role in proton translocation by allowing alternating access to aqueous channels (Stoeckenius, 1980) or by linking proton-conducting hydrogen-bonded amino acid side-group chains at either side of the membrane (Stoeckenius, 1977, 1980; Dunker, 1982; Nagle & Tristram-Nagle, 1983).

The presence of two spectroscopically similar M intermediates has been detected by several researchers using a variety of techniques. The second M intermediate has been seen at low temperatures with continuous illumination (Hess & Kuschmitz, 1977; Korenstein et al., 1978; Lozier et al., 1976) and also with flash spectroscopy (Ort & Parson, 1978; Ohno et al., 1981). In both of these approaches, measurement of the second M intermediate is possible because of the enhancement of the total population of M in the reaction mixture. Because this enhancement requires nonphysiological conditions that may modify the photochemical cycle (Stoeckenius & Bogomolni, 1982), techniques must be developed for examining the spectral intermediates in nonperturbing environments. Modulation excitation spectroscopy has been used to visualize two M_{412} intermediates with different lifetimes and polarizations in purple membrane fragments (Slifkin & Caplan, 1975). This technique has high sensitivity and, therefore, allows both intermediates to be easily detected under a wide variety of conditions. Intermediates can be distinguished by differences in kinetics and absorbance. This phase-modulation technique has been described elsewhere (Slifkin & Walmsley, 1970; Dewey & Hammes, 1981). Briefly, it consists of monitoring an intermediate by absorbance of a continuous light beam while driving the photocycle with an actinic light beam that is mechanically chopped. The absorbance will consequently be modulated at the same frequency as the actinic beam but will be phase-shifted due to the intermediate's finite lifetime. Kinetics of the intermediate can be determined from phase measurements or from the frequency dispersion of the signal amplitudes.

In this work a new application of phase-modulation spectroscopy is presented that allows the determination of structural parameters for photocycle intermediates. This technique employs the phase modulation of fluorescent energy transfer to locate the position of the retinal in the M intermediate state relative to fluorescent donors located on the membrane surface. From the measurement of fluorescence quenching and the measurement of the M_{412} concentration, the distance of the intermediate from the membrane surface label can be determined. The quenching of fluorescence due to energy transfer is measured with phase-sensitive detection when the actinic light is mechanically chopped. Since the lifetimes of the M_{412} intermediates are approximately 6 orders of magnitude slower

† This research was supported in part by NSF Grant PCM-8315263. C.A.H. is a Boettcher Foundation Fellow.

0006-2960/86/0425-0668$01.50/0

than the fluorescence lifetime, the fluorescence amplitudes measured in this experiment represent the steady-state quenching. An analysis of the amplitude of the fluorescent intensity as a function of modulation frequency shows that this signal is biphasic with lifetimes that correspond to the measured decay rates of the M intermediates. The M intermediate absorbance changes are measured on identical samples under identical conditions as the fluorescence measurements. The surface density of the M intermediate is varied by changing the chopping frequency of the actinic light. From the fluorescent amplitudes, the efficiency of fluorescence energy transfer to both the fast and the slow M intermediates can be calculated. With this fluorescence and absorbance information, the depth from the surface for both intermediates can be determined. Distances are measured for fluorescent probes located on the outer vesicular surface and for probes located on both surfaces. These results suggest that the retinal in the slow M intermediate is located significantly farther from the external vesicular surface than the fast M intermediate.

Materials and Methods

Chemicals. Asolectin (soybean phospholipid) was obtained from Associated Concentrates. Valinomycin and *n*-octyl β-D-glucopyranoside (octyl glucoside) were from Sigma. Lanthanum chloride was from Aldrich. 2-(Octadecylamino)-naphthalene-6-sulfonic acid (OANS)[1] was purchased from Molecular Probes. Solvents used were spectral grade, and all other chemicals were reagent-grade. All solutions were made in distilled, deionized water.

Purple Membrane and Reconstituted Vesicles. Halobacterium halobium S-9 was grown on defined media (Lanyi & MacDonald, 1979). Purple membrane fragments were purified with a sucrose step gradient (Becher & Cassim, 1975). Reconstituted vesicles were made by the octyl glucoside dilution technique (Racker et al., 1979). For vesicles with fluorescent label on both inner and outer surfaces, fluorescent-labeled lipid and asolectin in a ratio of 1:200 were dissolved in Me_2SO, and the solvent was evaporated in a test tube. Asolectin and Tricine buffer (50 mM Tricine, 0.15 M KCl, pH 8.0) were added to make a 20 mg/mL solution. The lipids were sonicated to clarity. Purple membrane was reconstituted into the sonicated vesicles by incubation on ice in the dark for 1 h in the presence of 1.15% octyl glucoside. The absorbance at 568 nm of bacteriorhodopsin in the reconstitution mixture was 1.0 OD. The octyl glucoside concentration was reduced by dilution of the sample over 100-fold in Tricine buffer with 5 mM added EDTA. The vesicles were concentrated by centrifugation at 110000*g* for 30 min and brought up in Tricine buffer with EDTA. Vesicles with fluorescent label only on the outer surface were prepared as above, except that the fluorescent lipid was added immediately before the experiments by adding microliter amounts of 5 mg of OANS/mL Me_2SO solution to the reconstituted vesicles while vortexing the mixture. Added Me_2SO never exceeded 1% of the total sample volume. Experiments were undertaken to ensure that dye added externally to vesicle preparations remained oriented on the outer membrane surface over the time period of our experiments. OANS was added to vesicle preparations by Me_2SO injection and allowed to incubate for periods up to 48 h. Quenching of OANS fluorescence by Cu^{2+} was used to assess the amount of fluorescent lipid on the vesicles' outer surface. Upon addition of 1.7 mM Cu^{2+} to a vesicle solution containing 7.4 μM incorporated OANS, the fluorescence decreased by 76%. This quenching varied by approximately ±7% over a 48-h time period. A second set of vesicles were exposed to the Cu^{2+} and were subjected to several freeze–thaw cycles. This process allows the Cu^{2+} to cross the lipid membrane. The fluorescence decrease in this case was identical with the initial decrease. These results suggest that the flipping of the label to the inner surface was extremely slow under the conditions of our experiment.

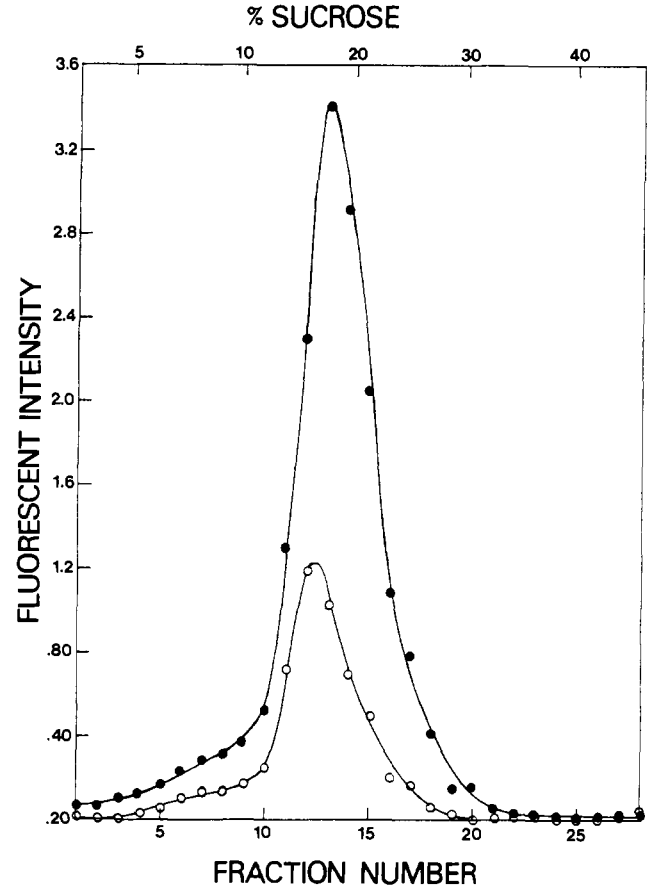

FIGURE 1: Fluorescence measurements of 1-mL fractions from 5 to 40% (w/w) sucrose density gradient containing asolectin vesicles reconstituted with bacteriorhodopsin and incorporated OANS fluorescent probe. The sample was centrifuged for 16 h at 55000*g*. Molar ratio of asolectin to BR is seen to be fairly homogeneous with respect to fraction number. Molar ratio of sample applied to the gradient was approximately 1700. (●) Fluorescence intensity (arbitrary units) of OANS dye, used to visualize location of asolectin. Excitation wavelength was 308 nm, and emission wavelength was 420 nm. (○) Fluorescence intensity (arbitrary units) of tryptophan, used to visualize location of bacteriorhodopsin. Spectra are corrected for presence of endogenous protein in asolectin. Excitation wavelength was 280 nm, and emission wavelength was 330 nm.

To assess the homogeneity of the vesicle preparations, reconstituted vesicles were centrifuged on a 5–40% (w/w) sucrose gradient for 16 h at 55000*g*. A single sharp band of vesicles was observed at approximately 18% sucrose. The protein concentration was determined by the bacteriorhodopsin's tryptophan fluorescence, and the fluorescent lipid was used to monitor the overall lipid content. The profiles of these two signals are shown in Figure 1. As can be seen from the figure, the lipid and protein profiles are similar. This shows that there is no unreconstituted protein or fluorescent probe and that all the vesicles are fairly homogeneous with respect to the protein-to-lipid ratio.

The bacteriorhodopsin in these vesicles has a net orientation opposite to the physiological orientation (Osterhelt &

[1] Abbreviations: OANS, 2-(octadecylamino)naphthalene-6-sulfonic acid; BR, bacteriorhodopsin; EDTA, ethylenediaminetetraacetic acid; Tricine, *N*-[tris(hydroxymethyl)methyl]glycine; DMPC, dimyristoylphosphatidylcholine; Me_2SO, dimethyl sulfoxide.

Stoeckenius, 1973; Lozier et al., 1976). In order to quantitate the fraction of protein oriented in this "inside-out" manner in the vesicles, the proton-pumping activity was measured in the absence and presence of 2.5 mM $LaCl_3$. Lanthanum displaces the divalent cations normally bound to the bacteriorhodopsin and inhibits proton transport (Chang et al., 1985; Drachev et al., 1981). This trivalent cation will be membrane-impermeable and can be used to selectively inhibit protein oriented to pump protons into the vesicles. By use of a proton-transport assay described previously (Racker & Stoeckenius, 1974), initial rates of inward proton transport of 2820 nmol of H^+ (mg of protein)$^{-1}$ min^{-1} were measured for the reconstituted vesicles at pH 7.4 in 2 M NaCl. Upon addition of lanthanum, no activity was present. For comparison, the same experiment was performed on freeze–thaw vesicles. These reconstituted vesicles were made according to the procedure of Kasahara & Hinkle, (1976) and have lower net proton-transport activity. In the absence of lanthanum, initial inward rates of 730 nmol of H^+ (mg of protein)$^{-1}$ min^{-1} were observed. Upon addition of La^{3+}, outward proton transport rates of 660 nmol of H^+ (mg of protein)$^{-1}$ min^{-1} were observed. This shows that the lanthanum was not crossing the membrane and inhibiting protein oriented with its cytoplasmic side on the inside of the vesicles. If it is assumed that both orientations should have the same initial transport rates, then the orientation of freeze–thaw vesicles is calculated to be 68% inside-out. The octyl glucoside dilution vesicles are virtually 100% oriented inside-out.

The surface density of the M_{412} intermediate in the asolectin vesicles was calculated from

$$\sigma = [875\ \text{Å}^2 + (875\ \text{Å}^2)C_{BR}/C_M + (68\ \text{Å}^2)C_L/(2C_M)]^{-1} \quad (1)$$

where C_{BR} and C_M are the molar concentration of bacteriorhodopsin and the M intermediate, respectively, and C_L is the molar concentration of lipid. The concentration of bacteriorhodopsin was determined spectroscopically with an extinction coefficient of 62 700 M^{-1} cm^{-1} at 568 nm (Rehorek & Heyn, 1979). The concentration of the M_{412} intermediate was calculated from the amplitude of the phase-modulated absorbance signals (see Results). The difference in the extinction coefficient between the M_{412} state and the ground state was used to calculate the M_{412} concentration. A value of 36 000 M^{-1} cm^{-1} was used (Becher et al., 1978). C_L, the concentration of asolectin, was determined from a M_r of 740 (Cerione et al., 1983). The surface area of a BR molecule on one vesicle surface was assumed to be 875 Å^2 (Henderson & Unwin, 1975), and the surface area of a lipid molecule was taken as 68 Å^2 (Huang & Mason, 1978). The factor of 2 in the denominator of the third term on the right-hand side of eq 1 arises because the lipids are distributed on both the inner and outer membrane surfaces.

Amplitude Measurements. The magnitude of the kinetic amplitudes of the M_{412} intermediate and of fluorescence quenching was measured on a modulation relaxation kinetic spectrometer similar to that described previously (Dewey & Hammes, 1981). A schematic of the instrument is shown in Figure 2. The photomultiplier that is collinear to the probe beam is used to measure the M_{412} absorbance signal. The second photomultiplier that is at a right angle to the probe beam measures the fluorescence of the donor. This design allows the measurement of both absorbance and fluorescence signals under identical conditions. Only the wavelength of the probe beam is changed in switching from the absorbance mode to the fluorescence mode. A PAR Model 5204 Lock-in analyzer was used to measure the amplitude of the absorbance or fluorescence signal. The probe beam was generated with a Schoeffel 150-W xenon arc lamp and an ISA Model H-20 monochrometer. Signals were detected on an EMI 9635 photomultiplier with a PPI 62/3A14 housing and preamp. The photomultiplier in the absorbance mode had a Corning 7-59 filter, and the photomultiplier in the fluorescence mode used a 2-in. focal-length lens and a Corning 5-57 filter. The excitation wavelength in the fluorescence mode was 305 nm. The actinic beam used an ELH 300-W lamp powered by a Lambda Model LK 344A DC power supply. This beam was chopped with an Ithaco Model 218 variable-speed chopper and was filtered with Corning CS 3-69 and I-75 filters. A 4.5-cm cell of saturated copper sulfate was also used as a filter. The variable-speed chopper generates a signal at the chopper frequency. This signal was used as the reference input for the lock-in amplifier. The frequency of the signal was measured with a Hewlett-Packard 5314 A universal counter. The temperature used in the experiments was 20 °C.

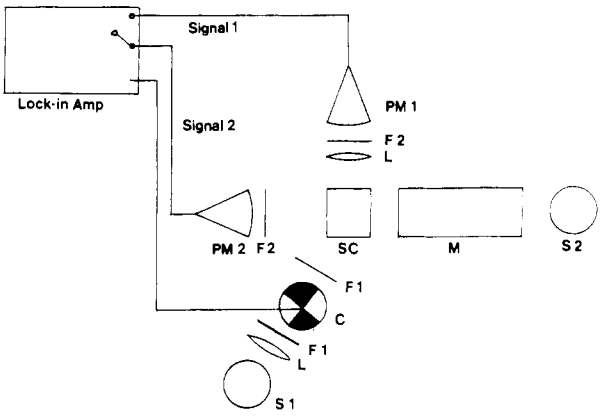

FIGURE 2: Schematic of the phase spectrophotometer used in these experiments. Orientation of the actinic source (S1) is perpendicular to the plane of the page. S2, monitoring beam; F1 and F2, cut-off filters; L, lens; C, mechanical chopper; SC, sample cell; M, monochrometer; PM1, photomultiplier monitoring fluorescence of sample; PM2, photomultiplier monitoring absorbance of sample.

Corrected spectra for determination of R_0 were measured on a Spex Fluorolog 2 series spectrofluorometer. To estimate errors in R_0, the fluorescence polarization of the OANS in asolectin vesicles was measured. A Perkin-Elmer Model MPF-3 spectrofluorometer was used for these polarization measurements. The steady-state fluorescence emission anisotropy r was measured as described previously (Fleming et al., 1979). This anisotropy is related to the averaged axial depolarization factor $\langle d_D \rangle$ by $\langle d_D \rangle = (r/0.4)^{1/2}$. This factor is then used to estimate errors in R_0 (Dale et al., 1979). All absorbance measurements were made on a Cary 219 spectrophotometer.

RESULTS

The concentration of the M_{412} intermediate was determined with the absorbance mode of the phase spectrophotometer and the equations:

$$C_M = \Delta A/\epsilon_M$$

$$\Delta A = A(\omega)/(A_{tot} \ln 10) \quad (2)$$

A_{tot} is the total voltage obtained from the absorbance photomultiplier in the absence of actinic light when the excitation monochrometer is set at 412 nm. $A(\omega)$ is the voltage of the absorbance amplitude measured using the phase-sensitive detector when chopped actinic light is directed on the sample cell. ϵ_M is the extinction coefficient of the M intermediate (see Materials and Methods). Typically, the concentration of the

M intermediate is less than 1% of the total bacteriorhodopsin concentration. The efficiency of energy transfer from the fluorescent lipid label to the retinal of the M_{412} intermediate is determined by

$$E = (Q_D - Q_{DA})/Q_D \quad (3)$$

where Q_D is the fluorescent quantum yield of donor in absence of acceptor and Q_{DA} is the fluorescent quantum yield in presence of acceptor. The total fluorescent signal obtained in the absence of actinic light is proportional to Q_D, and the fluorescent amplitude measured with the phase-sensitive detector in the presence of chopped actinic light is proportional to $Q_D - Q_{DA}$. The efficiency of resonance energy transfer in these experiments is quite small, being on the order of 10^{-4}. This low efficiency is observed above other quenching processes because the energy-transfer quenching is modulated by the photocycle and can be selectively detected by the phase-modulation technique. Nonmodulated quenching processes will not be detected. Care must still be taken that other quenching processes do not interfere. One possibility is modulated inner filter effects due to the absorbance changes of the photocycle. As a check on this, the photocycle absorbance signal was measured at the fluorescence excitation wavelength. No absorbance change was measured under the conditions of the fluorescence experiment, and therefore, inner filter effects are not a problem. A second possibility is that the formation of a membrane potential by the proton pump could modulate the spectral response of the fluorescent probe. Electrochroic effects due to the membrane potential have been commonly observed for the pigments in the chloroplast thylakoid [cf. Schmid et al. (1976)]. When valinomycin is added to our preparation to dissipate a membrane potential, there are small increases in both the M_{412} absorbance signal and in the fluorescent quenching signal. These changes compensate each other and indicate no net change in the parameters of the resonance energy-transfer process.

The frequency dependence of the M_{412} absorbance amplitude and the fluorescence amplitude are biphasic and can be fit by using the function:

$$A(\omega) = A_1 \tanh [\pi/(2\omega\tau_1)] + A_2 \tanh [\pi/(2\omega\tau_2)] \quad (4)$$

This function is the amplitude-response function for a square-wave perturbation. The form of this function is derived in the Appendix. A square-wave response function is used rather than the sinusoidal response function that appears in many applications of modulation spectroscopy [cf. Eigen & de Maeyer (1974)]. This is because the phase-sensitive detector used in this work "locks-in" on all the odd harmonics generated by the reference signal. Since the mechanical chopper generates a square wave and a square wave is made up entirely of odd harmonics, it is more appropriate to consider the perturbation caused by the actinic light to be a periodic square wave rather than a sine wave. To establish the validity of this analysis, we have measured the lifetimes for the decay of the M intermediates in purple membrane fragments. Our results are shown in Table I along with previous results from the literature. Good agreement is obtained with these previous results. An example of an amplitude dispersion for bacteriorhodopsin reconstituted into asolectin vesicles is shown in Figure 3. These results were fit to eq 4 by a nonlinear least-squares fitting routine. This routine provides values for the two amplitudes A_i and the two lifetimes τ_i. The fitted curve is shown in Figure 3 along with the fitted amplitudes of each component of the biphasic decay.

The fluorescent efficiencies and M_{412} intermediate surface densities are shown as a function of frequency in Figures 4 and 5. Data are shown for the case when the fluorescent label is located on the outer membrane surface and on both surfaces, respectively. The results of fitting these data to eq 4 are shown in Table I. As can be seen, the lifetimes of the fluorescence and absorbance signals are very similar. The fluorescence quenching due to energy transfer to the M state follows the decay of the M state because the fluorescent-transfer process is virtually instantaneous on this time scale.

In order to measure distances by resonance energy transfer, the characteristic Foerster distance R_0 must be determined for the specific donor acceptor pair under consideration. R_0 is defined as

$$R_0 = (Jk^2Q_Dn^{1/4})^{1/6}(9.7 \times 10^3 \text{ Å}) \quad (5)$$

where n is the refractive index of the medium, k^2 is an orientation factor characterizing the relative orientation of the transition dipoles of donor and acceptor, Q_D is the quantum

Table I: M_{412} Intermediate Kinetics

protein state	method	τ_1 (ms)	τ_2 (ms)	$A_2/(A_1 + A_2)$
purple membrane	phase[a]	14.8	3.9	0.08
	phase[b]	11.7	4.5	0.21
	phase[c]	13.5	3.0	
	flash[d]	9.2	3.8	0.26
	flash[e]	15.0	2.5	0.37
BR monomers in vesicles (absorbance)	phase	77.8[f]	10.6[f]	0.37
		77.6[g]	10.9[g]	0.41
BR monomers in vesicles (fluorescence)	phase	61.4[f]	9.2[f]	0.30
		64.3[g]	9.8[g]	0.52

[a] pH 7.85, distilled water and conditions as in reference in footnote *d*. [b] pH 8.00, 0.15 M KCl, 50 mM Tricine. Same conditions as vesicles. [c] Slifkin et al., 1978. [d] Lozier et al., 1976. Each half-life taken from this paper was converted to a relaxation time. Amplitude ratio was estimated from reference's Figure 4. [e] Tristram-Nagle & Packer, 1981. [f] Both vesicle surfaces labeled with OANS. [g] Outer vesicle surface labeled with OANS.

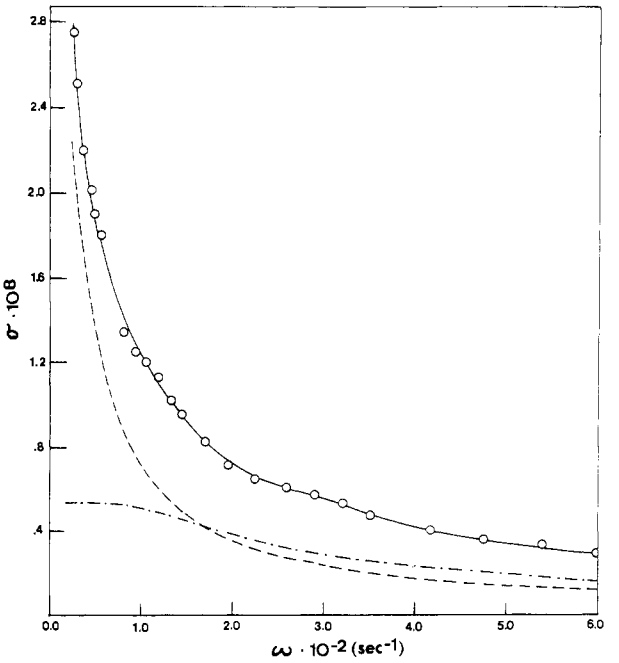

FIGURE 3: Amplitude dispersion for bacteriorhodopsin reconstituted into asolectin vesicles. The experimental amplitude vs. frequency data were analyzed by a nonlinear least-squares fit, which yielded two amplitudes and two lifetimes. By use of these values and eq 4 of the text, the frequency dependence of the surface densities for the slow and fast M intermediates could be plotted. The fitted curve shown is the sum of these individual curves.

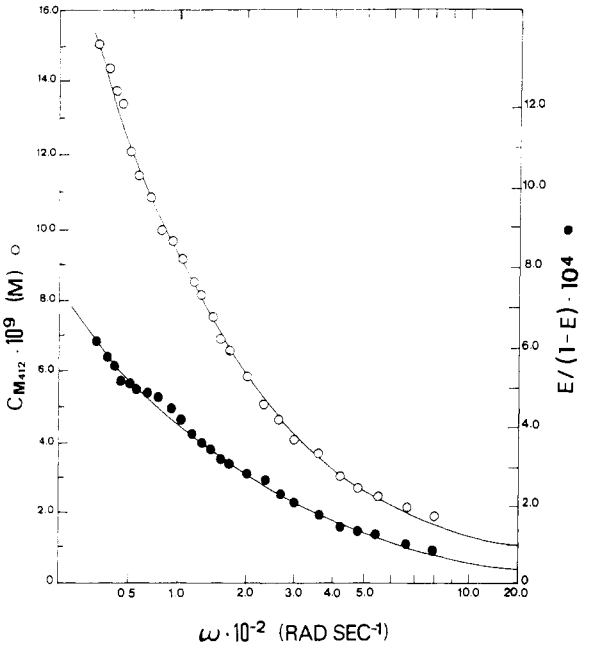

FIGURE 4: Plot of total concentration of the M intermediates (○) and energy-transfer efficiency (●) vs. frequency of modulation of actinic light for bacteriorhodopsin incorporated into asolectin vesicles. OANS label is present on outer vesicle surface only. Theoretical curve (—) is obtained by summing curves obtained for slow and fast M components when data are fit to eq 4 by a nonlinear least-squares fitting routine.

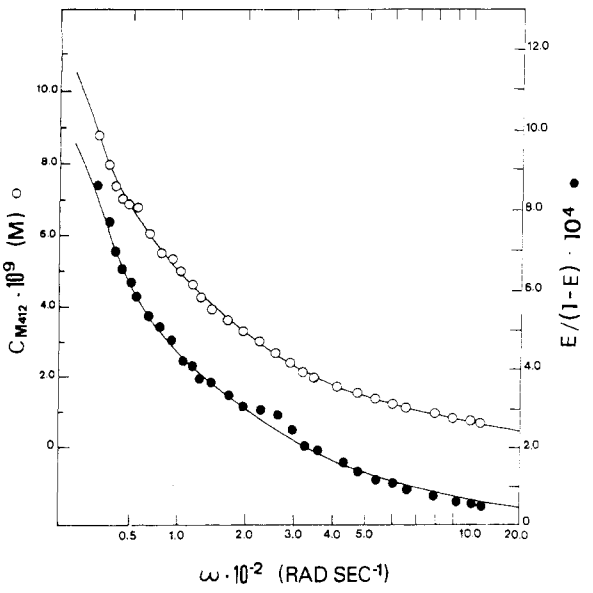

FIGURE 5: Plot of total concentration of the M intermediates (○) and energy-transfer efficiency (●) vs. frequency of modulation of actinic light for bacteriorhodopsin incorporated into asolectin vesicles. OANS label is present on both vesicle surfaces. Theoretical curve as obtained in Figure 4.

yield of the donor, and J is a measure of the overlap of the fluorescence spectrum of the donor and the absorbance spectrum of the acceptor. The refractive index was taken to be that of hexane, which is 1.38 (*CRC Handbook of Chemistry and Physics*, 1978–1979). This value was used because the transfer distances occur through the lipid bilayer. Refractive indices do not change dramatically from one media to the next, and R_0 is not a sensitive function of refractive index. Using the refractive index for water instead of hexane changes R_0 by less than 1%. k^2 was taken to be $^2/_3$, which assumes free relative rotation of donor and acceptor. This assumption is

Table II: Distances from OANS to Retinal of M Intermediates

condition	intermediate	L_1 (Å)[a]	L_2 (Å)[b]
OANS on outer vesicle surface	slow	36.5	38.2
	fast	27.4	32.2
OANS on both vesicle surfaces	slow	27.3	26.8
	fast	29.8	28.8
OANS on inner vesicle surface	slow		28.7[c]
	fast		37.2[c]

[a] Calculated from fitted amplitudes for efficiencies and surface densities for each intermediate. [b] Calculated using bilinear least-squares fit of fluorescence data. [c] Calculated from outer surface data and both surface data using eq 8 of the text.

discussed in detail under Discussion. The OANS quantum yield was measured in asolectin vesicles against a standard (quinine sulfate in 1.0 N H_2SO_4, $Q = 0.70$ at 340 nm) by the method of Chen (1967). The overlap integral J was calculated from the fluorescent emission spectrum for OANS and the absorbance spectrum for the M intermediate determined by Lozier and co-workers (Lozier et al., 1975) and by Ebrey and co-workers (Becher et al., 1978). These spectra represent a composite of the spectra for the two intermediates. By use of these two different spectra, which were determined under very different conditions, R_0 values of 50.7 and 48.7 Å were determined, respectively. The 50.7-Å value obtained from Lozier's spectrum was used throughout. These results suggest that R_0 is not highly sensitive to the small differences observed in the spectra for the M state. Previous work suggests that the spectra for the two M_{412} intermediates are very similar (Korenstein et al., 1978; Ohno, 1981). Therefore, identical R_0 values were used for the two M states. A potential source of error in R_0 is in the value used for the extinction coefficient for the M_{412} intermediates. However, R_0^6 is directly proportional to the extinction coefficient and σ_{M412} is inversely proportional to it. Therefore, the calculated distances are actually independent of the extinction coefficient (cf. eq 6).

Distances of closest approach for the slow and fast M_{412} intermediates were obtained in two ways. First, the fitted amplitudes for the efficiencies and for the surface densities of both intermediates were used to calculate the distance from the surface to each intermediate. Bacteriorhodopsin reconstituted into asolectin vesicles was used at temperatures where the BR is present in monomers (Dencher et al., 1983). For the two-dimensional case in the limit of low surface density of acceptor, the distance of closest approach of a donor to an isolated acceptor molecule is given by (Shaklai et al., 1977; Dewey & Hammes, 1980)

$$L = [(\pi/2)R_0^6\sigma_A[E/(1-E)]^{-1}]^{1/4} \quad (6)$$

where L is the distance of closest approach, σ_A is the fitted amplitude for the surface density of acceptor, and E is the fitted amplitude for the efficiency of energy transfer. The values obtained for L by this method are given in Table II. Because the fluorescence signals obtained in these experiments are very weak, considerable error can be introduced with the four-parameter fit to eq 4 in the calculation of L. Therefore, the fluorescence data were analyzed directly with a bilinear model. The observed efficiency E is related to the surface density of the M intermediates by

$$E(\omega)/[1 - E(\omega)] = m_s\sigma_s(\omega) + m_f\sigma_f(\omega) \quad (7)$$

where $m_s = \pi R_0^6(2L_s^4)^{-1}$ and $m_f = \pi R_0^6(2L_f^4)^{-1}$. Plots of $E/(1 - E)$ vs. σ_{M412} are shown in Figure 6 for the case where the fluorescent donor is present on both vesicle surfaces and for the case where the donor is present on one vesicle surface only. The $E/(1 - E)$ vs. σ_A plots are clearly nonlinear and cannot be adequately fit with a linear model. The data were accu-

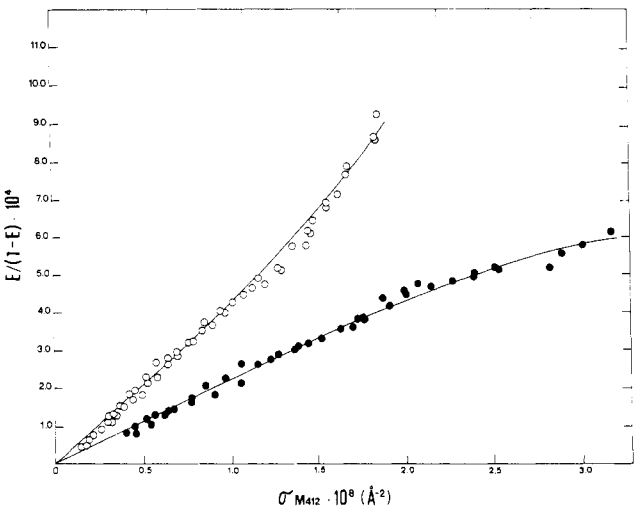

FIGURE 6: Plot of efficiency of energy transfer from OANS probe to M intermediate vs. M intermediate surface density in asolectin vesicles. Energy transfer from outer surface of vesicles only (●); energy transfer from inner and outer vesicle surfaces (○). Data points represent results of two experiments for each set of conditions. The fitted curves were obtained as follows: Surface densities for each component were found by fitting the absorbance data to eq 4. These calculated values were then used in a bilinear least-squares fit of eq 7, which yielded values for m_s and m_f.

rately fit with the bilinear model described by eq 7. The σ_{M412} value for each component was determined from fitting the absorbance data to eq 4. These calculated values for σ_{M412} were then used in a bilinear least-squares fit of eq 7. The parameters m_f and m_s were determined from this bilinear fit. The fitted lines are shown in Figure 6. From the values of m_s and m_f, the distances L_s and L_f are determined. L_s and L_f values obtained in this manner are comparable to those obtained by the first method of analysis, but the magnitudes of differences between distances are more consistent from experiment to experiment when eq 7 is used. As can be seen from Table II, for vesicles labeled on both surfaces, the slow component appears approximately 2 Å closer to the donor than the fast component. When only one surface is labeled, the fast component appears approximately 6 Å closer to the donor. Absolute distances for L_s and L_f may vary within 20% from experiment to experiment, but the relative difference in distances for both the one-surface and two-surface cases does not change. The energy-transfer efficiency from both surfaces is the sum of energy-transfer efficiency from each surface. Therefore

$$L^{-4}(\text{two surfaces}) = L^{-4}(\text{outer surface}) + L^{-4}(\text{inner surface}) \quad (8)$$

Thus, the distance of closest approach from each M_{412} intermediate to a donor molecule on either side of the membrane can be determined. These distances are shown in Table II and represented diagrammatically in Figure 7.

DISCUSSION

By using phase modulation of fluorescence energy transfer we have been able to measure changes in the position of the retinal during the photocycle of bacteriorhodopsin. This technique uses phase-sensitive detection to determine the concentration of a photocycle intermediate and the resulting fluorescence quenching due to energy transfer. This work demonstrates significant differences in location of the chromophore relative to the membrane surface for each M state (see Figure 7). This information will be helpful in evaluating possible reaction mechanisms involving two M intermediates.

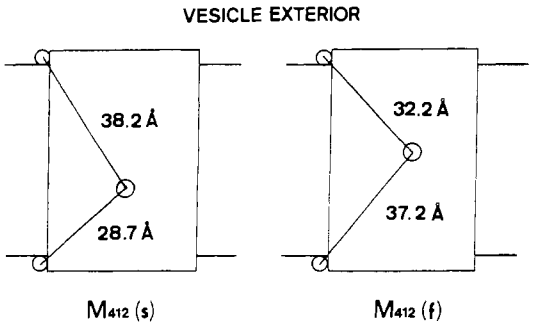

FIGURE 7: Diagram of distances from each vesicle surface to retinal in the slow- and fast-decaying M intermediates. Distances are measured from the center of the fluorescent probe OANS located at the membrane surfaces.

Before considering the interpretation of the results for energy transfer to the M_{412} intermediates of bacteriorhodopsin, we first discuss the assumption involved in measuring distances by this technique. As in most applications of fluorescence energy transfer, the main uncertainty arises in determining the value for the characteristic Foerster distance R_0. This is because of uncertainties in the orientation factor k^2. In the present work a value for k^2 of $^2/_3$ is used. This is the appropriate value when the relative orientation of donor and acceptor is averaged by rapid rotational motion. The uncertainty in the orientation factor may be estimated with fluorescent polarization information (Dale et al., 1979). This method may be applied to the case of two-dimensional energy transfer (Wolber & Hudson, 1979). Ideally, the fluorescent polarization of the donor and acceptor can be measured as well as the polarization of the transfer process. In this work the fluorescent polarization of the donor OANS was measured. The anisotropy factor r was found to be 0.041. This low value is representative of a fluorescent probe in a lipid bilayer above its phase-transition temperature (Heyn, 1979). If the donor anisotropy value is used and no assumptions are made about the polarization of the M states, the error in the measured distances can be estimated [Figure 9 of Dale et al. (1979)]. Under these conditions, the error in the measured distances is greater than 20%. However, it is likely that the retinal is rotationally averaged. Unfortunately, it would be extremely difficult to measure the fluorescent polarization of emission from the M state because this state is not highly fluorescent. Data obtained from the polarization of the weak fluorescence of ground-state retinal in purple membrane (Kouyama et al., 1985) and from absorbance anisotropy (Razi Naqvi et al., 1973; Sherman et al., 1976; Korenstein & Hess, 1978) suggest that the retinal is immobilized in the protein. In our experiments, bacteriorhodopsin is in its monomeric state, and the major contribution to the rotational motion of the retinal arises from the rotation of the entire protein. This rotational motion is very fast for reconstituted, monomeric bacteriorhodopsin. The time-resolved, absorption anisotropy $r(t)$ has been measured for bacteriorhodopsin reconstituted in DMPC vesicles at 25 °C (Cherry et al., 1977). $r(t)$ decays from a limiting initial value above 0.1 to a value of 0.037 in less than 0.5 ms. This limiting value of 0.037 is indicative of rapid rotational motion of the protein about an axis normal to the membrane. Since the lifetimes of the M states are much longer than this rotational relaxation process, the orientation of the retinal in the M state is averaged by the fast rotation of the protein. The effect of the rotation of the protein in the membrane on the orientation factor has been considered in previous theoretical work (Koppel et al., 1979). By use of eq 22 in Koppel et al. (1979) and eq 24 and Figure 9 in Dale et al. (1979), these

rotational effects on the orientation factor may be calculated. By assuming that the retinal is rigidly held (anisotropy factor of 0.4) and by use of the anisotropy factor of 0.039 for protein rotation, uncertainties in k^2 were determined. The resulting uncertainty in the distance was ±9%. This represents the major source of error since the uncertainty in the experimental measurement is ±1%. Our results as shown in Figure 7 show differences in the distances for the two intermediates. Because of the uncertainties in k^2, a portion of these apparent distance changes may be due to changes in the orientation of the chromophore in the two states. However, the distances determined from the inner vesicle membrane surface are outside the range of uncertainty and clearly indicate a change in location for the two states. In future work, distances will be measured from a variety of donor probes. This should help establish the origin of the apparent distance change.

In the present analysis, the experimentally determined absorbance amplitudes are assumed to be directly related to the concentration of the chemical intermediates. However, the relaxation amplitude represents a normal mode of the chemical reaction and does not necessarily represent the concentration amplitude of a single, reaction intermediate. The distances that are measured with this technique must then be considered as distances to the normal reaction mode and not to a specific chemical species. They will represent a complicated weighted average of the distances to the chemical species involved in the specific normal mode. This normal mode average will then be intermediate in value between those of the individual chemical species. Thus, the differences in distance between the slow and fast reaction modes of the M_{412} decay will represent a lower limit for the distance between the two M_{412} intermediate species involved. It is conceivable that only one M species is present in the photocycle (Parodi et al., 1984). If other photocycle species contribute to the observed amplitudes, the observed distances would reflect differences in the locations of these intermediates. On the time scale of this experiment, the ground state of bacteriorhodopsin would probably make the major contribution. If only a single M state exists, it must then be at a significantly different location from the ground state. To obtain a distance to a given species, one must first determine the contributions of each species to the normal mode. This can be done by assuming a specific reaction mechanism. Since no specific reaction mechanism has been generally agreed upon for the photocycle of bacteriorhodopsin, this analysis has not been carried out. A normal-mode analysis of a variety of different mechanisms will be examined in a future paper. In the present work, we shall use our distances to determine lower limits for the difference in position of the two intermediates.

Our results show relatively large distance changes for the retinal during the photocycle. It has previously been proposed that the retinal in the M intermediate undergoes considerable rotational motion (Sherman & Caplan, 1977). While a large change in retinal orientation could cause much of our observed, apparent distance changes, such a mechanism cannot totally account for the entire change. Our results are consistent with a net translation of the retinal within the protein. The distances that are observed in this experiment are the distance of closest approach from a lipid donor at the membrane surface to the retinal acceptor in the M state. This closest approach will represent an average of the distances from the periphery of the protein on the membrane surface to the retinal buried in the protein. This distance could change during a conformational process by the retinal attached to the lysine residue acting as a swinging arm. This swinging motion would result

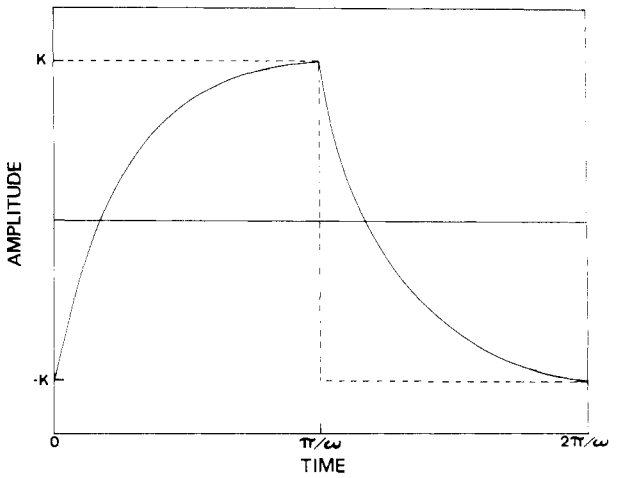

FIGURE 8: Diagram of the square-wave periodic perturbation amplitude (dotted line) and the exponential, chemical relaxation response function (solid line) vs. time. Time is in units of reciprocal frequency.

in both a rotation and a net translation of the retinal. Another possibility is that the protein could fan out on the membrane surface and push the lipid further away from a relatively static retinal. This may be accomplished by changes in the tilt of the α-helical barrels of the bacteriorhodopsin. The swinging-arm model is consistent with the different polarization of the two M components observed by Slifkin & Caplan (1975). However, the fact that the absorbance characteristics of the two M intermediates are so similar (Korenstein et al., 1978; Ohno et al., 1981) indicates no dramatic change in retinal's local environment. This result would be more consistent with the protein-fanning model. Recently, circular dichroism spectra have been obtained for the M intermediate (Draheim & Cassim, 1985). The M_{412} spectrum shows large changes relative to ground-state bacteriorhodopsin in all regions of the spectrum. These results were interpreted as an indication of large-scale global conformational changes. This is consistent with the relatively large changes that are observed in this work. Although the molecular basis for the chromophore movement seen in this study is not known, these results demonstrate the dynamic, flexible nature of bacteriorhodopsin as it proceeds through its photocycle.

This technique is easily adapted to other membrane-bound protein systems where dynamic processes are accompanied by conformational changes. Systems that are activated by a membrane potential or chemiosmotic gradient may be coupled to the light-driven proton-pumping process of bacteriorhodopsin or to the light-driven chloride pump of halorhodopsin. Thus, this technique has potential application to a wide range of membrane-bound transport proteins. Since most conformational processes are on a millisecond time scale, there should be no problem with the time resolution of the technique. Driving the acceptor concentration by frequency modulation of the actinic light provides an easy and convenient method for determining the dependence of energy transfer on surface density of acceptor. At these extremely low acceptor surface densities the difficult theoretical analysis of two-dimensional energy transfer (Wolber & Hudson, 1979; Dewey & Hammes, 1981; Snyder & Friere, 1982) reduces to a simple, accurate analytic expression (Shaklai et al., 1977; Dewey & Hammes, 1981). Thus, some of the difficulties that hamper energy-transfer measurements in membrane systems are avoided by this technique. Future work will investigate energy transfer from fluorescent probes at a variety of locations in the lipid bilayer. This should help resolve any ambiguities inherent when a single donor–acceptor pair is used and better

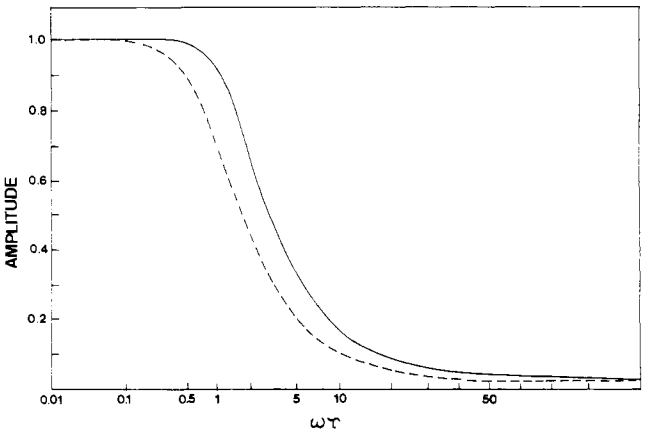

FIGURE 9: Comparison of the frequency dispersion of the relaxation response function to a periodic square-wave perturbation (solid line) and to a periodic sinusoidal perturbation (dotted line).

characterize the observed distances for the M state.

ACKNOWLEDGMENTS

We thank J. Krupinski and Dr. G. G. Hammes for valuable discussions on methods of characterization of the reconstituted vesicles.

APPENDIX

Frequency Response to a Periodic Square-Wave Perturbation. Many phase-sensitive detectors will use the principal harmonic of the reference signal to "lock-in" on the input signal. Such detectors will respond to the sinusoidal perturbation of the principal harmonic of a square wave forcing function. The response to a light-driven process that is modulated with a mechanical chopper (square wave) will then be the same as a sinusoidal perturbation. The measured amplitude A as a function of frequency ω is given by (Eigen & de Maeyer, 1974)

$$A = \sum_i A_i/(1 + \omega\tau_i)^{1/2} \qquad \text{(A1)}$$

where the sum is over the normal modes of the chemical relaxation process and τ_i is the relaxation time of the ith normal mode. The sinusoidal response function will be phase-shifted by the phase angle ϕ_i and

$$\tan \phi_i = \omega\tau_i \qquad \text{(A2)}$$

These expressions are commonly used to analyze the frequency response in a modulation relaxation experiment (Slifkin, 1968; Dewey & Hammes, 1981). Some lock-in amplifiers such as the PAR 5204 used in this work will respond to all the odd harmonics of the reference signal. Since the Fourier components of a square wave consist entirely of odd harmonics, it would be inappropriate to consider the perturbation to be sinusoidal. In this appendix the stationary forced relaxation response to a square-wave perturbation is derived. We closely follow the formalism of Eigen & de Maeyer in our derivation of the amplitude dispersion function. It is assumed that the dependent, observable variable y responds linearly to the perturbation. In this case the perturbation is the periodic forcing function $\bar{y}$. The stationary forced solution to the first-order differential equation

$$\tau(dy/dt) + y = \bar{y} \qquad \text{(A3)}$$

is given by

$$y_{\text{forced}} = \int_0^t \tau^{-1} \exp[-(t - \theta)/\tau]\bar{y}(\theta)\, d\theta \qquad \text{(A4)}$$

In the present treatment, we consider only a single relaxation mode. The square-wave forcing function is

$$\bar{y} = (4K/\pi)\sum_{n=0}^{\infty}(2n + 1)^{-1} \sin [(2n + 1)\omega t] \qquad \text{(A5)}$$

where K is the square-wave amplitude (see Figure 8). Substituting eq A5 into eq A4 and integrating gives

$$y_{\text{forced}} = (4K/\pi)\sum_{n=0}^{\infty}\{[(2n + 1)\omega^2\tau^2]^{-1} \sin [(2n + 1)\omega t] - (\omega\tau)^{-1} \cos [(2n + 1)\omega t]\}/[(\omega\tau)^{-2} + (2n + 1)^2] \qquad \text{(A6)}$$

This expression may be further simplified with the series (Mangulis, 1965):

$$\sum_{n=0}^{\infty}\frac{\cos [(2n + 1)\theta]}{(2n + 1)^2 + x^2} = \frac{\pi \sinh [x(\pi/2 - \theta)]}{4x \cosh (\pi x/2)} \qquad 0 \le \theta \le \pi \qquad \text{(A7)}$$

By taking the indefinite integral of eq A7 with respect to θ, one can show that

$$\sum_{n=0}^{\infty}\frac{\sin [(2n + 1)\theta]}{(2n + 1)[(2n + 1)^2 + x^2]} = \frac{-\pi \cosh [x(\pi/2 - \theta)]}{4x^2 \cosh (\pi x/2)} \qquad 0 \le \theta \le \pi \qquad \text{(A8)}$$

These relationships can be used during the positive cycle of the square wave; $0 \le t \le \pi/\omega$. For the negative cycle, $\pi/\omega \le t \le 2\pi/\omega$, one needs

$$\sum_{n=0}^{\infty}\frac{\cos [(2n + 1)\theta]}{(2n + 1)^2 + x^2} = \frac{\pi \sinh [x(\pi/2 + \theta)]}{4x \cosh (\pi x/2)} \qquad \pi \le \theta \le 2\pi \qquad \text{(A9)}$$

$$\sum_{n=0}^{\infty}\frac{\sin [(2n + 1)\theta]}{(2n + 1)[(2n + 1)^2 + x^2]} = \frac{-\pi \cosh [x(\pi/2 - \theta)]}{4x^2 \cosh (\pi x/2)} \qquad \pi \le \theta \le 2\pi \qquad \text{(A10)}$$

which can be derived from eq A7 and A8 with basic trigonometric relations. Using these relationship, eq A6 is simplified to give

$$y_{\text{forced}} = \frac{-Ke^{\pi/2\omega\tau}e^{-t/\tau}}{\cosh (\pi/2\omega\tau)} \qquad 0 \le t \le \pi/\omega \qquad \text{(A11)}$$

$$y_{\text{forced}} = \frac{Ke^{-\pi/2\omega\tau}e^{-t/\tau}}{\cosh (\pi/2\omega\tau)} + \text{const} \qquad \pi/\omega \le t \le 2\pi/\omega$$

Thus, the response function is a simple exponential during both the on and off cycles (see Figure 8). The total amplitude of the cycle A is given by

$$A = y_{\text{forced}}(\pi/\omega) - y_{\text{forced}}(0) \qquad \text{(A12)}$$

$$A = 2K \tanh (\pi/2\omega\tau)$$

This is the function used in the previous paper to determine the lifetime of the relaxation process from the frequency dependence of the amplitudes. For multiple processes, the amplitude will be a summation of all normal-mode amplitudes:

$$A = \sum_i 2K_i \tanh (\pi/2\omega\tau_i) \qquad \text{(A13)}$$

In Figure 9 the amplitude dispersion for the square-wave perturbation (eq A12) is compared with the one for a sinusoidal wave (eq A1 for $i = 1$). A comparison of experimental results obtained with eq A13 to literature values for the kinetics of the decay of the M intermediate of purple membrane is

presented in the previous paper.

Registry No. Retinal, 116-31-4.

REFERENCES

Aton, B., Doukas, A. G., Callender, R. H., Becher, B., & Ebrey, T. G. (1977) *Biochemistry 16*, 2995–2999.

Becher, B. M., & Cassim, J. Y. (1975) *Prep. Biochem. 5*, 161–178.

Becher, B. M., Tokunaga, F., & Ebrey, T. G. (1978) *Biochemistry 17*, 2293–2300.

Campion, A., El-Sayed, M. A., & Terner, J. (1977) *Biophys. J. 20*, 369–375.

Cerione, R. A., McCarty, R. E., & Hammes, G. G. (1983) *Biochemistry 22*, 769–776.

Chang, C.-H., Chen, J.-G., Govindjee, R., & Ebrey, T. (1985) *Proc. Natl. Acad. Sci. U.S.A. 82*, 396–400.

Chen, R. (1967) *Anal. Biochem. 19*, 374–387.

Cherry, R. J., Mueller, U., & Scheider, G. (1977) *FEBS Lett. 80*, 465–468.

CRC Handbook of Chemistry and Physics (1978–1979) Vol. 59, p C-333, CRC Press, Boca Raton, FL.

Dale, R. E., Eisinger, J., & Blumberg, W. E. (1979) *Biophys. J. 26*, 161–194.

Dencher, N. A., Kohl, K.-D., & Heyn, M. P. (1983) *Biochemistry 22*, 1323–1334.

Dewey, T. G., & Hammes, G. G. (1980) *Biophys. J. 32*, 1023–1035.

Dewey, T. G., & Hammes, G. G. (1981) *Proc. Natl. Acad. Sci. U.S.A. 78*, 7422–7425.

Drachev, A. I., Drachev, L. A., Kaulen, A. D., & Khitrina, L. V. (1984) *Eur. J. Biochem. 138*, 349–356.

Draheim, J. E., & Cassim, J. Y. (1985) *Biophys. J. 47*, 497–507.

Dunker, A. K. (1982) *J. Theor. Biol. 97*, 95–127.

Eigen, M., & de Maeyer, L. (1974) *Tech. Chem. (N.Y.) 6*, 63–146.

Fleming, P. J., Koppel, D. E., Lau, A. L., & Strittmatter, P. (1979) *Biochemistry 18*, 5458–5464.

Henderson, R., & Unwin, P. N. T. (1975) *Nature (London) 257*, 28–32.

Hess, B., & Kuschmitz, D. (1977) *FEBS Lett. 74*, 20–23.

Heyn, M. P. (1979) *FEBS Lett. 108*, 359–364.

Huang, C., & Mason, J. (1978) *Proc. Natl. Acad. Sci. U.S.A. 75*, 308–310.

Kasahara, M., & Hinkle, P. C. (1976) *Proc. Natl. Acad. Sci. U.S.A. 73*, 396–400.

Koppel, D. E., Fleming, P. J., & Strittmatter, P. (1979) *Biochemistry 18*, 5450–5457.

Korenstein, R., & Hess, B. (1978) *FEBS Lett. 89*, 15–20.

Korenstein, R., Hess, B., & Kuschmitz, D. (1978) *FEBS Lett. 93*, 266–270.

Kouyama, T., Kinosita, K., & Ikegami, A. (1985) *Biophys. J. 47*, 43–54.

Lanyi, J. K., & MacDonald, R. E. (1979) *Methods Enzymol. 56*, 398–407.

Lewis, A., Spoonhower, J., Bogomolni, R. A., Lozier, R., & Stoeckenius, W. (1974) *Proc. Natl. Acad. Sci. U.S.A. 71*, 4462–4466.

Lozier, R. H., Bogomolni, R. A., & Stoeckenius, W. (1975) *Biophys. J. 15*, 955–962.

Lozier, R. H., Niederberger, W., Bogomolni, R. A., Hwang, S.-B., & Stoeckenius, W. (1976) *Biochim. Biophys. Acta 440*, 545–556.

Mendelsohn, R. (1976) *Biochim. Biophys. Acta 427*, 295–301.

Nagle, J. F., & Tristram-Nagle, S. (1983) *J. Membr. Biol. 74*, 1–14.

Ohno, K., Takeuchi, Y., & Yoshida, M. (1981) *Photochem. Photobiol. 33*, 573–578.

Ort, D. R., & Parson, W. W. (1978) *J. Biol. Chem. 253*, 6158–6164.

Osterhelt, D., & Stoeckenius, W. (1973) *Proc. Natl. Acad. Sci. U.S.A. 70*, 2853–2857.

Parodi, L. A. (1984) *Photochem. Photobiol. 40*, 501–512.

Racker, E., & Stoeckenius, W. (1974) *J. Biol. Chem. 249*, 662–663.

Racker, E., Violand, B., O'Neal, S., Alfonzo, M., & Telford, J. (1979) *Arch. Biochem. Biophys. 198*, 470–477.

Razi Naqvi, K., Rodriguez, J. G., Cherry, R. J., & Chapman, D. (1973) *Nature (London), New Biol. 245*, 249–251.

Rehorek, M., & Heyn, M. P. (1979) *Biochemistry 18*, 4977–4983.

Schmid, R., Shavit, N., & Junge, W. (1976) *Biochim. Biophys. Acta 430*, 145–153.

Shaklai, N., Yguerabide, J., & Ranney, H. M. (1977) *Biochemistry 16*, 5585–5592.

Sherman, W. V., & Caplan, S. R. (1977) *Nature (London) 265*, 273–275.

Sherman, W. V., Slifkin, M. A., & Caplan, S. R. (1976) *Biochim. Biophys. Acta 423*, 238–248.

Slifkin, M. A., & Walmsley, R. H. (1970) *J. Phys. E. 3*, 160–162.

Slifkin, M. A., & Caplan, S. R. (1975) *Nature (London) 253*, 56–58.

Slifkin, M. A., Garty, H., & Caplan, S. R. (1978) in *Energetics and Structure of Halophilic Microorganisms* (Caplan, S. R., & Ginzberg, M., Eds.) pp 165–184, Elsevier, New York.

Snyder, B., & Freire, E. (1982) *Biophys. J. 40*, 137–148.

Stoeckenius, W. (1977) *J. Gen. Physiol. 70*, 23a.

Stoeckenius, W. (1980) *Acc. Chem. Res. 13*, 337–44.

Stoeckenius, W., & Bogomolni, R. A. (1982) *Annu. Rev. Biochem. 52*, 587–616.

Tristram-Nagle, S., & Packer, L. (1981) *Biochem. Int. 3*, 621–628.

Wolber, P. K., & Hudson, B. S. (1979) *Biophys. J. 28*, 197–210.